Interdigital Oil Droplets Sensor with Acoustic Enabled Pre-Positioning

Xiaoyue Jiang

Electrical Engineering and Computer Sciences
University of California at Berkeley

Technical Report No. UCB/EECS-2015-92
http://www.eecs.berkeley.edu/Pubs/TechRpts/2015/EECS-2015-92.html

May 14, 2015

Interdigital Oil Droplets Sensor with Acoustic Enabled Pre-Positioning

by

Xiaoyue (Joy) Jiang

B.S. (University of Rochester) 2013

A report submitted in partial satisfaction of the

requirements for the degree of

Master of Science

in

Electrical Engineering and Computer Science

in the

Graduate Division

of the

University of California, Berkeley

Committee in charge:

Professor Albert P. Pisano, Chair
Professor Liwei Lin

Spring 2015

Interdigital Oil Droplets Sensor with Acoustic Enabled Pre-Positioning

by

Xiaoyue (Joy) Jiang

Research Project

Submitted to the Department of Electrical Engineering and Computer Sciences, University of California at Berkeley, in partial satisfaction of the requirements for the degree of **Master of Science, Plan II**.

Approval for the Report and Comprehensive Examination:

Committee:

Professor Albert P. Pisano
Research Advisor

(Date)

* * * * * * *

Professor Liwei Lin
Second Reader

(Date)

Interdigital Oil Droplets Sensor with Acoustic Enabled Pre-Positioning

Xiaoyue (Joy) Jiang

Abstract

Interdigital Oil Droplets Sensor with Acoustic Enabled Pre-Positioning

by

Xiaoyue (Joy) Jiang

Master of Science in Electrical Engineering and Computer Sciences

University of California, Berkeley

Chair Albert P. Pisano

Oil content in the ocean needs to be monitored for the human beings to track the health of our marine ecosystem as well as to take any early action regarding natural seeps and human-made oil spills. Sensitive, robust, reliable, and low power sensors are needed to establish sensor network in the ocean for high temporal and spatial resolution oil content monitoring.

This work investigates a micro scale interdigital sensor that enables long-duration monitoring of oil droplets and water-in-oil emulsions. An acoustic wave field enabled pre-positioning of oil droplets was proposed and evaluated.

The proposed micro scale interdigital sensor showed a simulated limit of detection of around 4 ppm. And the effects of the electrode spacing, amount of oil droplets, and droplet size, position, and dielectric properties on sensor performance were characterized. Lastly, an acoustic wave field enabled pre-positioning of oil droplets were proposed and investigated to eliminate the performance variation due to the position and distribution of oil droplets.

_____

Professor Albert P. Pisano

Research Advisor

Table of Contents

List of Figures

List of Tables

List of Symbols and Abbreviations

$A_{electrode}$	Area of the Electrode Surface, m^2
c_i	Concentration of Species *i*, mol/m^3
C	Capacitance, F
C_b	Bulk Capacitance, F
ε	Electrical Permittivity, F/m
ε_0	Vacuum Permittivity, 8.854×10^{-12} F/m
ε_{eff}	Effective Dielectric Constant
ε_b	Dielectric Constant of the Bulk Solution
ε_w	Dielectric Constant of Water
ε_m	Dielectric Constant of the Medium
E_{ac}	Acoustic Energy, J
F	Faraday's Constant, 96487 C/equiv
F_{rad}	Acoustic Radiation Force, N
κ	Cell Constant, 1/m
k	Wave Vector, rad/m
N	Number of Electrodes
L	Length of Electrodes, m
P_0	Pressure Amplitude, m
R	Universal Gas Constant, 8.314 J/mol K
R_b	Bulk Resistance, Ω

R_p	Radius of the Particle, m
T	Absolute Temperature, K
t_{aco}	Maximum Time for Particle Manipulation, s
V	Volume of the Particle in the Medium, m^3
V_w	Volume Fraction of the Water in Water-in-Oil Emulsion
ν	Kinematic Viscosity, m^2/s
ω	Angular Frequency, rad/s
z	Ionic Valence
Y_{tot}	Total Admittance, S
β_m	Compressibility of the Medium
β_p	Compressibility of the Particle
δ	Momentum Diffusion Layer, m
σ	Conductivity, S/m
λ	Ultrasonic Wavelength, m
λ_D	Debye Length, m
ρ_m	Density of the Medium, Kg/m^3
ρ_p	Density of the Particle, Kg/m^3
Φ	Acoustic Contrast Factor

Chapter 1: Introduction

1.1 Fate of Oil Spill

The U.S. National Research Council of the National Academy of Sciences estimates that the worldwide average annual release of petroleum is 1.3 million tonnes, which is equivalent to the consumption of about 832,000 cars per year [1]. The four major sources of input include natural seeps (46%), discharges from consumption of oils (37%), accidental spills from ships (12%), and extraction of oil (3%) [1]. Oil content in the ocean needs to be monitored for the human beings to track the health of our marine ecosystem as well as to take any early action regarding natural seeps and oil spills. And the recent Deepwater Horizon disaster has raised discussions on how to develop the oil spill science and technology for responses to future events.

Crude oil consists mostly of paraffin, naphthenes, and aromatics, which are composed mainly of hydrogen and carbon. Once crude oil spills into the sea, it will go through spreading, evaporation, dispersion, emulsification, dissolution, sedimentation, and biodegradation [1]. A schematic of the weathering process are shown in Figure 1. Among all the process, dispersion starts soon after the spill and reaches a maximum rate at about 10 hours after an accident [2]. During this process, oil droplets with an average radius of 35 μm are formed under the shear forces from waves and turbulence, where the smaller droplets remain in suspension in the sea [2]. Meanwhile, the process of emulsification leads to stable semi-solid residuals, and it has been shown that droplets with 15 μm radiuses do not degrade at a depth of 1000 to 2000 meter in the ocean [3].

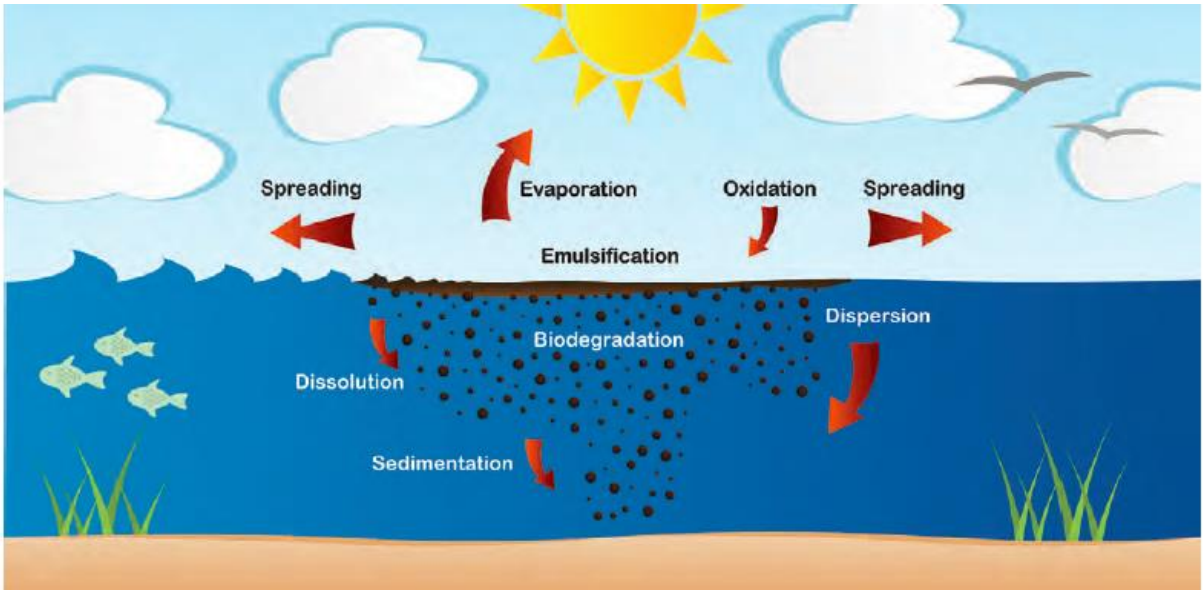

Figure 1. A schematic of all the weathering process, adapted from ITOPF [2].

1.2 Monitoring of the Oil Spill

In order to be prepared with a quick and proper response, an accurate assessment of the spreading of the oil is needed. Normally, modeling the oil spill weathering behavior and real time monitoring are used together for this assessment.

In terms of modeling, the environmental conditions, time-dependent physical and chemical properties, and chemical and physical mechanisms of oil weathering must be fully understood and incorporated into the model with real time data [4].

On the other hand, real time monitoring of the oil has been achieved with engineered instrumentations. Remote sensing, including using optical sensors, laser fluorosensors, microwave sensors, slick thickness determination, acoustic systems, integrated airborne sensor systems, and satellite remote sensing, have been widely adapted and thoroughly reviewed in literature [5]. Table 1 shows the sensitivity of some of the methods, where

most of the methods are only able to identify oil spill once a layer of hydrocarbon is formed.

	Infrared	Ultraviolet Fluorometer	Laser Fluorosensors	Visual
Sensitivity	10-70 μm layer	0.01 ppb	10 μm layer	0.05 μm layer

Table 1. Sensitivity of some of the Oil Spill Remote Sensing Methods [5]

At the same time, the instruments that are capable of analyzing the size and presence of the oil droplets in situ are limited in researching the motion of the oil droplets in the ocean. A laser in situ scattering and transmissometry system (LISST-100X, Sequoia Scientific Inc. Seattle, WA) has been reported as one of the successful systems set up in the laboratory of research vessels [6]. While the other reported instrument is HoloPOD (Holographic Plankton Observation Device), which could take images and measurements of similarly tiny oil droplets [7].

The instruments to measure the concentration of oil in the produced water have also provided the overall category of the oil sensing mechanism. Infrared absorption, gravimetric as well as gas chromatography, and flame ionization detection (GC-FID) are the three main types of reference methods [8]. The techniques for bench-top or online instruments are colorimetric, fiber optical chemical sensor, infrared, UV absorption, UV fluorescence, focused ultrasonic acoustics, image analysis, light scattering and turbidity, and photoacoustic sensor [8].

1.3 Sensor Network in the Ocean for Oil Monitoring

In recent years, underwater wireless sensor networks has been investigated as a promising area for development of ocean-observation systems, where both the deployment and sensor technology are sufficiently mature to motivate the idea of

underwater sensor networks. Figure 2 illustrates some of the ways to deploy an underwater sensor network. One of the potential applications enabled by sensor networks in the ocean is a chemical in situ sensor with high temporal and spatial resolution of measurements and high duration deployments.

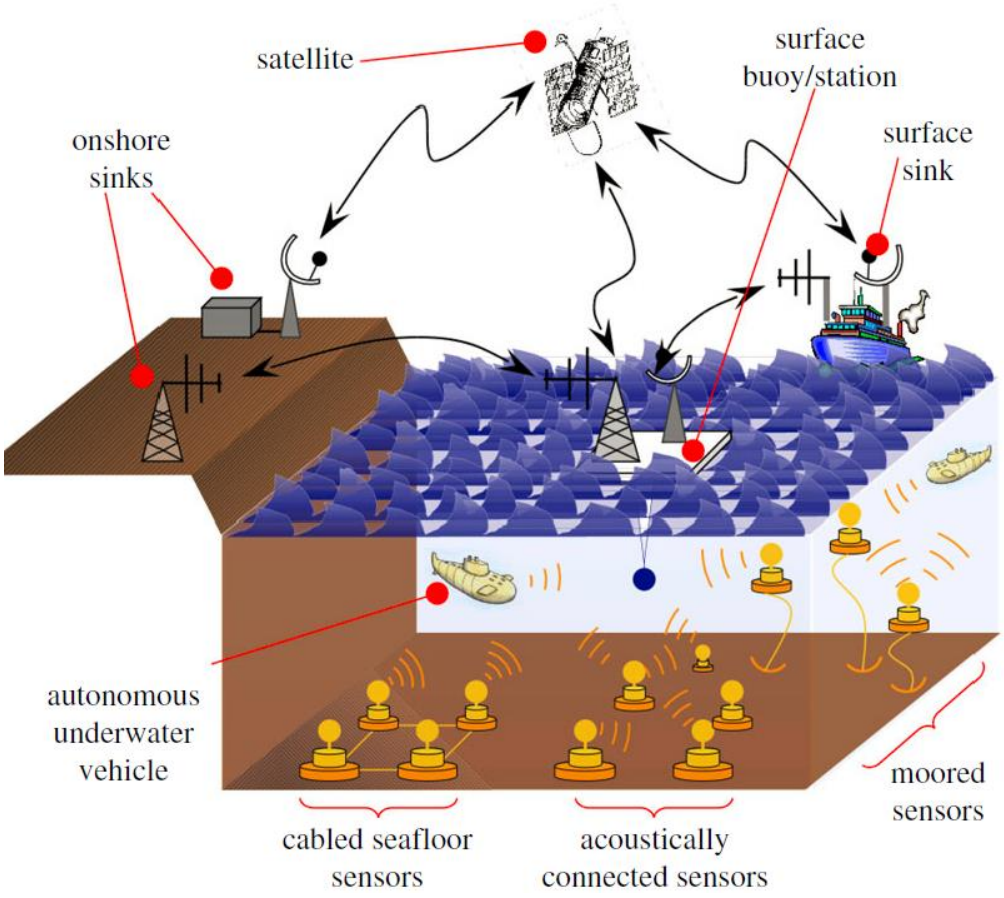

Figure 2. Ways to deploy an underwater sensor network, adapted from Heidemann et al. [9]

In terms of oil spill monitoring, sensor network architectures for monitoring underwater pipelines have been demonstrated [10]. Moreover, algorithms for using wireless sensor networks to locate the source of an underwater oil spill have been developed [11].

1.4 Interdigitated Electrode Sensors

Interdigital electrodes, shown in Figure 3, are periodic electrode structures commonly used in sensors and actuators. The miniaturization of interdigitated electrodes has been demonstrated as a low cost sensor array for non-destructive materials evaluation, whose application includes humidity sensors, monitoring of cure processes, piezoelectric SAW devices, and capacitive sensor arrays.

Figure 3. A layout of interdigitated electrodes patterned on a substrate

1.5 Droplets Manipulation and Positioning

The emerging field of droplet based microfluidics has led to extensive research on droplet manipulation with magnetic, centrifugal, hydrodynamic, electrokinetic, and dielectrophoretic forces. However, these methods require a micro scale channel, which is not suitable for droplet manipulation and positioning in *in vivo* real time sensing applications. But the research in recent years on micro droplets manipulation and patterning in acoustic wave field has shed light on positioning and manipulation micro oil droplets. In these applications, the acoustic wave was generated by an acoustic resonator incorporating piezoelectric transducers.

1.6 Research Objective and Thesis Organization

This work investigates a micro scale interdigital sensor that enables long-duration monitoring of oil droplets and water-in-oil emulsions, and that can be implemented in sensor network in the ocean for applications requiring high temporal and spatial resolution. This report consists of five chapters. Chapter 1 introduces the motivation and current technologies for monitoring oil content in the ocean. Chapter 2 lists the fundamentals of the analytical solution to the equivalent circuit of interdigital sensors as well as the basics for acoustic radiation force. Chapter 3 focuses on the analysis, simulation, and results of the proposed interdigital sensors. Chapter 4 reports the potential of using acoustic wave field for oil droplets pre-positioning. Chapter 5 concludes the work and discusses future work.

Chapter 2: Background

2.1 Electrical Properties of Oil and the Seawater

Hydrocarbons are dielectrics with an average dielectric constant from 2.1 to 2.4, and a conductivity of 10^{-9} S/m. When hydrocarbons disperse in water, water-in-oil emulsions will form and remain as stable semi-solid spherical droplets. Compared with saline solutions, water-in-oil emulsions have a distinctive dielectric constant based on the volume fraction of water in oil, following the Maxwell Garnett mixing formula [12]. The Maxwell Garnett mixing formula approximate the effective dielectric constant ε_{eff} based on the dielectric constant of the medium ε_m and that of the inclusion ε_w, in this case, the water, as following

$$\frac{\varepsilon_{eff} - \varepsilon_m}{\varepsilon_{eff} + 2\varepsilon_m} = V_w\left(\frac{\varepsilon_w - \varepsilon_m}{\varepsilon_w + 2\varepsilon_m}\right) \tag{2.1}$$

where V_w is the volume fraction of the water in oil. And the Maxwell Garnett equation is solved by [13]:

$$\varepsilon_{eff} = \varepsilon_m\left(\frac{2V_w(\varepsilon_w - \varepsilon_m) + \varepsilon_w + 2\varepsilon_m}{\varepsilon_w + 2\varepsilon_m - V_w(\varepsilon_w - \varepsilon_m)}\right) \tag{2.2}$$

And the electrical properties of sea water are a function of the temperature and salinity, where the conductivity is about 5 S/m at a salinity of 30 g/Kg at 25 ˚C [14]. And the dielectric constant of sea water is similar to that of water, which is 78.

2.2 Basics of the Circuit Modeling for Interdigital Electrode

Circuit Modeling for Planar Interdigitated Electrodes

A cell constant κ is defined for planar interdigitated electrodes to help electrodes design, where

$$\kappa = \frac{2}{NL} \tag{2.3}$$

for N electrodes with a length of L [15]. Then the resistance in the bulk solution between the electrodes R_b is

$$R_b = \frac{\kappa}{\sigma} \tag{2.3}$$

and the capacitance for the bulk solution between the electrodes C_b is

$$C_b = \frac{\varepsilon_b \varepsilon_0}{\kappa} \tag{2.4}$$

where σ is the conductivity, ε_0 is the vacuum permittivity, ε_b is the dielectric constant of the bulk solution [15].

Electric Double Layer

At the interface of electrodes and conducting electrolyte, an electric double layer will form once the electrical potential is applied on the electrode. At the solid-liquid interface, the free ions near the electrode will experience both electrostatic forces and Brownian agitation. The Gouy-Chapman model has derived the ion and potential distribution near the surface of the electrode. By combining Boltzmann statistics with Poisson equation, Poisson-Boltzmann equation is derived and solved. And a characteristic length, defined as Debye length λ_D, can be used to measure how the overpotential decays from the

electrode surface into the bulk. A schematic of the Gouy-Chapman model is shown in Figure 4. And the Debye length is given by

$$\lambda_D = \sqrt{\frac{\varepsilon RT}{2z^2F^2c_\infty}} \tag{2.5}$$

for a single salt of symmetric ionic valences ($z_+ = -z_- = z$), where ε is the electrical permittivity, R is the universal gas constant, T is the absolute temperature, z is the ionic valence, F is the Faraday's constant, and c_∞ is concentration of the bulk solution [16].

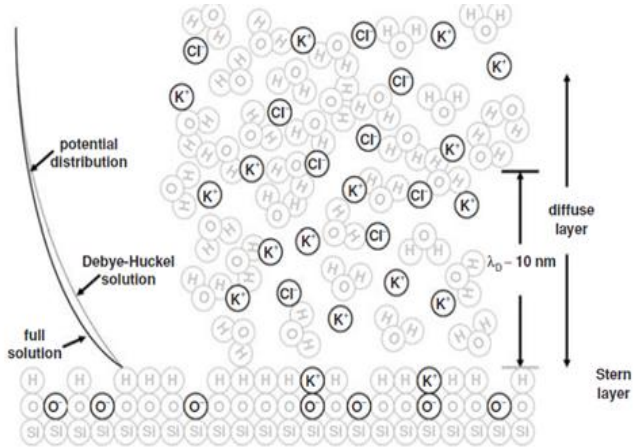

Figure 4. A schematic of the Gouy-Chapman model, adapted from Kirby [16]

This interface can be idealized and approximated as a capacitor. Where the interface capacitance can be roughly approximated as

$$C = \frac{\varepsilon_b \varepsilon_0 A_{electrode}}{\lambda_D} \tag{2.6}$$

where C is the capacitance and $A_{electrode}$ is the area of the electrode surface [16].

However, Gouy-Chapman model has treated the ions and solvent as ideal, namely a dilute solution of point charges. But other work has been done to show the equivalent circuit model for a thin double layer does not break down until enormous voltage is applied in a concentrated solution [17].

Penetration Depth

The penetration depth is to characterize the distance of the effective electric field on top of the planar electrode. The penetration depth of the electric field above these interdigital electrodes, demonstrated in Figure 5, is proportional to the spacing between the centerlines of the sensing and the driven electrodes [18]. And the penetration depth defines the affective sensing distance above the electrodes.

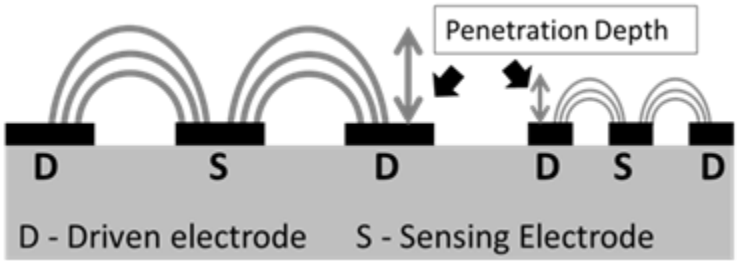

Figure 5. Schematic of the penetration depth

2.3 Acoustic Radiation Force

When a layer of liquid is in contact with a piezoelectric transducer, the pressure fluctuations will be transmitted from the substrate to the fluid medium and establish an acoustic pressure field above the substrate. This acoustic pressure field will lead to an acoustic radiation force on the droplets suspended in this fluid medium above the substrate. This acoustic radiation force is a result of the non-linear components of the pressure field from acoustic waves. In previous research, L.V. King, L.P. Gor'Kov, and H. Bruus have derived the analytical solution to the acoustic radiation force F_{rad} in an inviscid fluid being [19]

$$F_{rad} = -(\frac{\pi p_o^2 V_p \beta_m}{2\lambda})\Phi(\beta,\rho)\sin(2kx) \tag{2.7}$$

with

$$\Phi(\beta,\rho)=\frac{5\rho_p-2\rho_m}{2\rho_p+\rho_m}-\frac{\beta_p}{\beta_m} \tag{2.8}$$

and

$$E_{ac}=\frac{p_o^2}{4\rho_m c_m{}^2} \tag{2.9}$$

where P_0 is the pressure amplitude, V the volume of the particle in the medium, λ the ultrasonic wavelength, k the wave vector, x the distance from an anti-pressure node to a pressure node, ρ the density, Φ the acoustic contrast factor, β the compressibility, E_{ac} the acoustic energy respectively. The subscripts of *p* and *m* indicate particle and medium, respectively. As shown in Figure 6, a particle with positive acoustic contract factor in an acoustic field will be subject to acoustic radiation force to move from the pressure nodes until it reaches the equilibrium point. The derivation of this set of equations has ignored the thermal and viscous effects on the droplets. This assumption is only valid when the radius of the particle R_p of interest is smaller than the wavelength λ and larger than the momentum diffusion layer δ, which is defined as

$$\delta=\sqrt{\frac{2\upsilon}{\omega}} \tag{2.10}$$

where ν is the kinematic viscosity and ω is the angular frequency of the acoustic field. The momentum diffusion layer is calculated to be around 0.6 μm for a 1-MHz ultrasound in water at room temperature [19]. And the analysis of the speed of droplets manipulation is done in J Guo's work [20]. Guo has derived the maximum time t_{aco} for the particle with radius R_p to move from a pressure node to the equilibrium point being

$$t_{aco}=\frac{9\pi\nu\rho_m}{\Phi E_{ac}}\frac{\ln[\cot(kR_p)]}{2\pi(kR_p)^2} \tag{2.11}$$

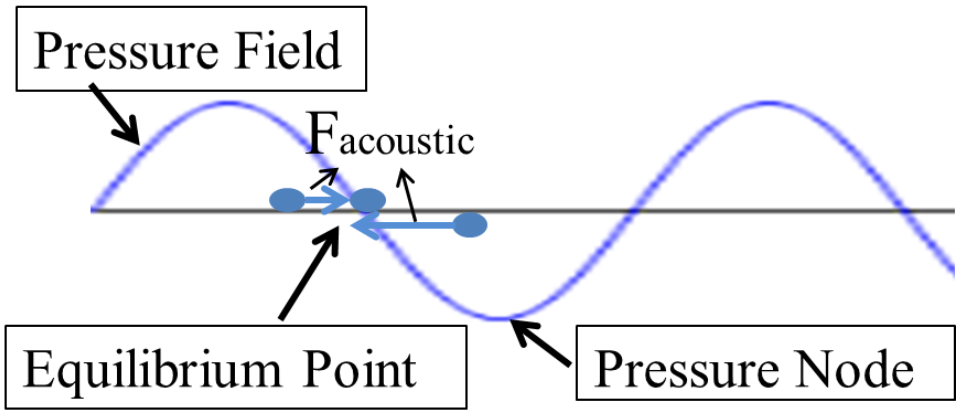

Figure 6. The motion of a particle with positive acoustic contract factor in an acoustic field

Chapter 3: Interdigital Sensor for Oil Droplets Detection

3.1 Analytical Solution and Simulation Setup

When calculating the analytical solution, the interdigitated electrodes were modeled to be on a glass substrate and in direct contact with the bulk solution, shown in Figure 7. Only two electrodes, one for driving and one for sensing, were considered. Here the bulk solution was assumed to be 0.599 mmol/L sodium chloride solution corresponding to a salinity of 35g/kg. In this model, a layer of electric double layer was assumed to form when an electrical potential is applied at the electrodes. Therefore, eight electric elements were used for the equivalent circuit, including resistance and capacitance in the bulk, substrate, and at the interface between the bulk solution and substrate. In this case, the electric double layer was modeled as ideal resistors and capacitors in series with the electrical elements in the bulk solution. And the total resistance and capacitance of the bulk solution and interface were in parallel with that of the substrate. Here, C_b , R_b , C_{dl} , R_{dl} , R_s , and C_S , labeled in Figure 7, were the resistance and the capacitance for the bulk fluid under test, electrical double layer, and the substrate respectively. And the total admittance Y_{tot} was calculated as:

$$Y_{tot} = \left[\left(\left(\frac{1}{2R_{dl}} + \frac{1}{\frac{1}{2j\omega C_{dl}}} \right)^{-1} + \left(\frac{1}{R_B} + \frac{1}{\frac{1}{j\omega C_B}} \right)^{-1} \right)^{-1} + \left(\frac{1}{R_s} + \frac{1}{\frac{1}{j\omega C_s}} \right) \right] \tag{3.1}$$

where ω is the angular frequency and $j = \sqrt{-1}$.

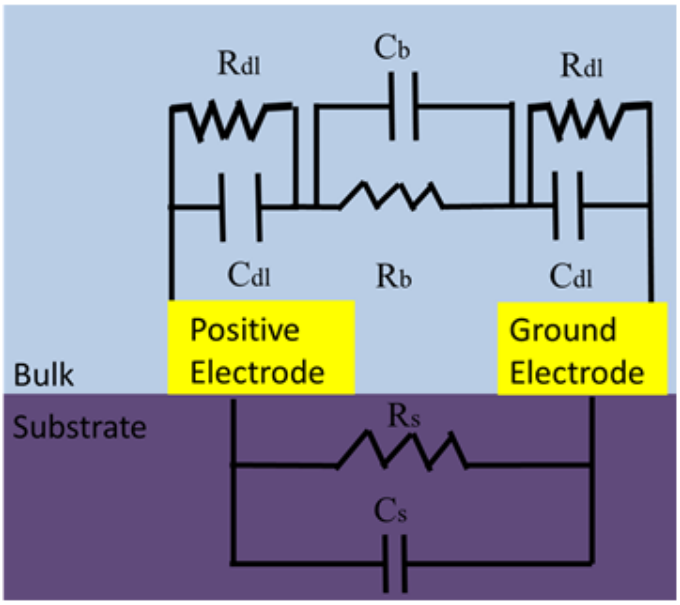

Figure 7. Schematics of all the electrical elements for the analytical model

The AC/DC Module in COMSOL Multiphysics was used for simulation. The 2D geometries used for the case without oil droplet is shown on the left of Figure 8, and the case with oil droplet is shown on the right of Figure 8. Five domains, including sea water, electrode, substrate, electric double layer, and oil droplet, were used for the case with oil droplet. And only four domains, previous domains without the one for oil droplet, were used for the case without oil droplet. The admittance between two electrodes with half of the electrode length on the device was simulated, since the electrodes were repetitive structures. And the spacing between the inner edges of the two electrodes was always the same as one electrode width, which made the distance between the centers of the electrodes twice as the electrode width. And a domain of electrical double layer is implemented for an accurate presentation of the physical phenomenon. The materials and electrical properties of different domains were listed in Table 2.

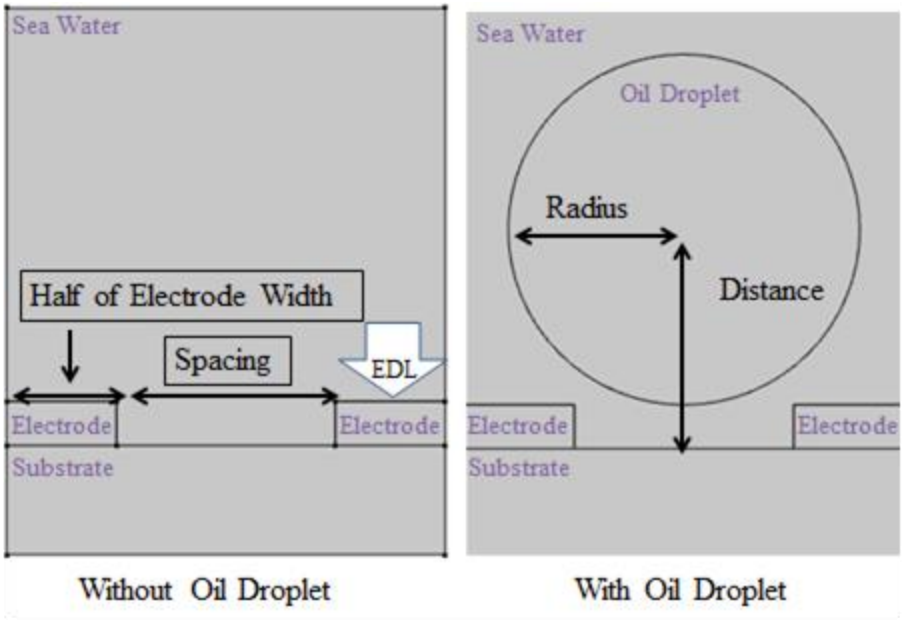

Figure 8. Geometries used in the AC/DC Module in COMSOL Multiphysics for the case without oil droplet (left) and with an oil droplet (right)

Domain	Material	Electrical Conductivity [S/m]	Dielectric Constance
Sea Water	0.599 mmol/L sodium chloride solution	5	80
Electric Double Layer		2.7×10^{-9}	339
Electrode	platinum	10^{7}	1
Substrate	glass	10^{-14}	4.5
Oil	hydrocarbon	10^{-9}	78

Table 2. Materials with Their Electrical Properties for Different Domains in Simulation

First of all, no oil droplets between two 10 μm wide electrodes were modeled, illustrated on the left of Figure 8, whose simulation results were verified with analytical solution. The analytical solution to the admittance between the electrodes was computed from Equation 2.3-2.6, and the values for individual electrical components were listed in Table 3. The comparison is plotted in Figure 9, which shows the simulation is relative consistent with the analytical solution. The difference comes from the fact that the simulated electrodes in COMSOL have finite thickness. To verify the effect of the finite

thickness of the electrodes, 5 μm, 10 μm, and 15 μm thick electrodes were simulated. The admittances between 10 μm wide electrodes with different thickness from 10^3 to 10^8 Hz are shown in Figure 10. As the thickness of the electrode increases, the admittance at higher frequencies increases. This is because as the thickness of the electrodes increases, the width of the direct path of the current between the electrodes increases, which leads to an increase in admittance. And since the theory assumes perfect planar electrodes, the finite thickness of the electrodes in simulation will lead to an increase in the admittance. At this point, the discrepancy between the results from the analytical solution and the simulation was well explained, which has verified the simulation as a reliable method to characterize this system.

Electrical Elements	Value
Resistance in Electric Double Layer (R_{dl})	$7.4\times10^{8}\ \Omega$
Capacitance in Electric Double Layer (C_{dl})	4.42×10^{-7} F
Resistance in Bulk Solution (R_b)	$0.4\ \Omega$
Capacitance in Bulk Solution (C_b)	3.54×10^{-11} F
Resistance in Substrate (R_s)	$2\times10^{9}\ \Omega$
Capacitance in Substrate (C_s)	1.77×10^{-11} F

Table 3. Values for Individual Electrical Elements from Analytical Solution

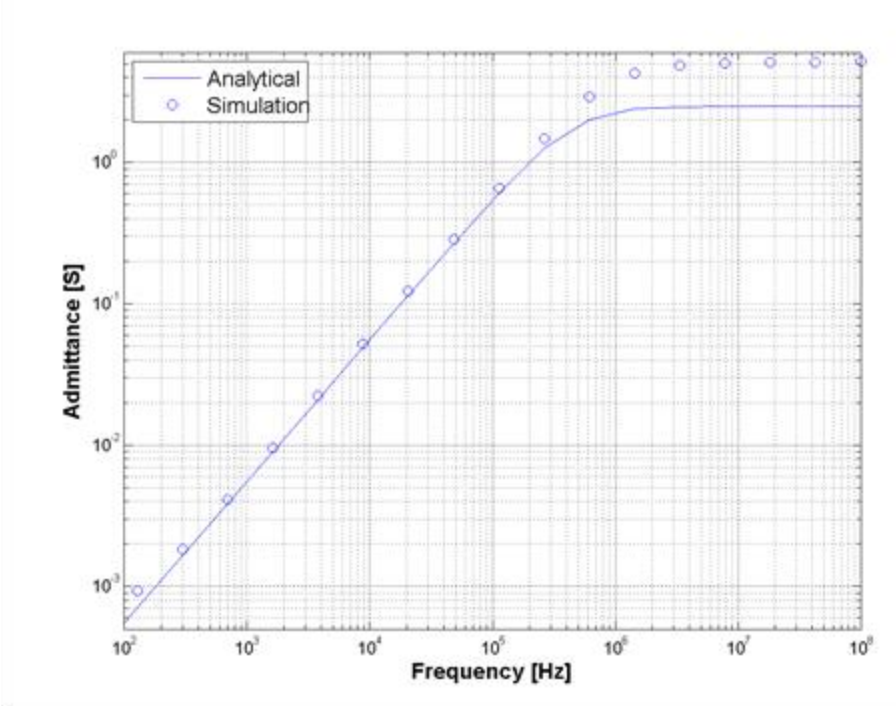

Figure 9.Comparison of the simulated and analytical solutions to the admittance between two electrodes from 10^2 to 10^8 Hz for 10 µm width and 5 µm thick electrodes

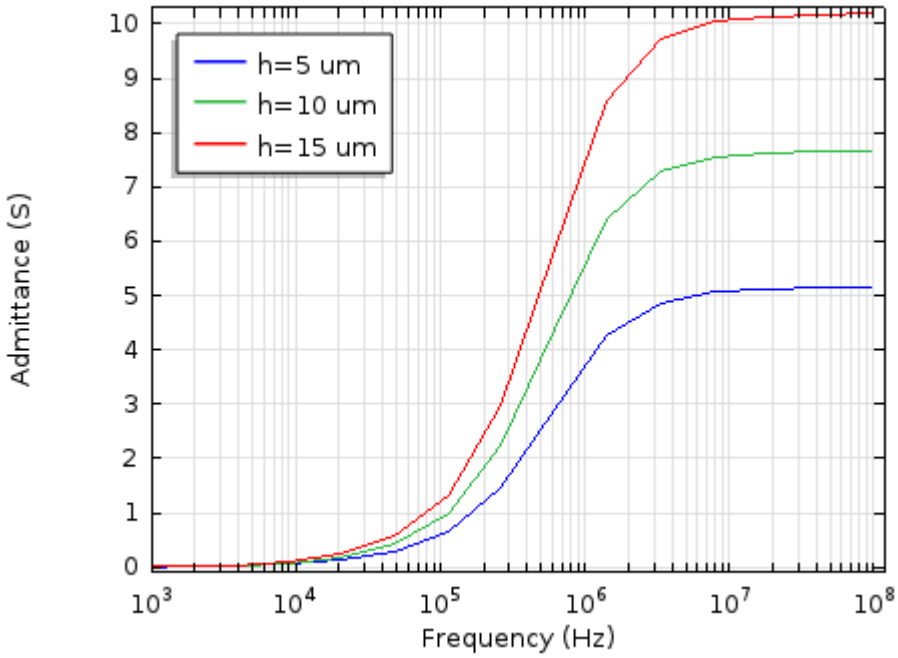

Figure 10.Comparison of the admittance between 10 µm wide electrodes from 10^3 to 10^8 Hz for electrode thickness of 5, 10, and 15 µm.

3.2 Penetration Depth

How the penetration depth changes respect to the frequency and the width of the electrodes were investigated to understand the effective sensing area. The simulated electrical potential distribution at 10 Hz and 10^8 Hz are shown in Figure 11. This meant high frequency signals are needed if any electrical responses to oil droplet in the sea water are desired. This is because of the presence of the electrical double layer, where the electrical double layer leads to a low admittance at low frequency and high admittance at high frequency. Therefore, at low frequency, the current prefer to go through the substrate rather than through the sea water. The electrical potentials at different frequencies above the 10 μm wide positive electrodes into the seawater are shown in Figure 12. The results suggest frequencies between 10^6 to 10^8 Hz are needed for 10 μm wide electrodes during sensing if a penetration depth of around 10 μm is desired.

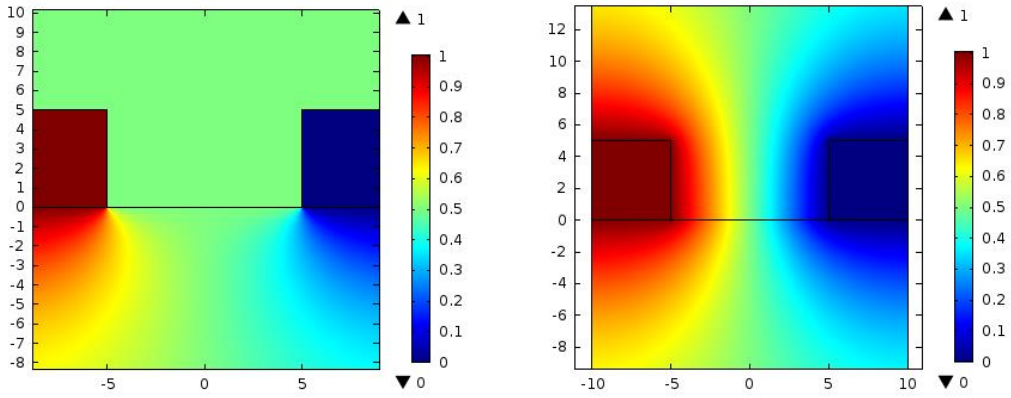

Figure 11.Electrical potential distribution for10 Hz (left) and 10^8 Hz (right) for 10 μm wide electrodes

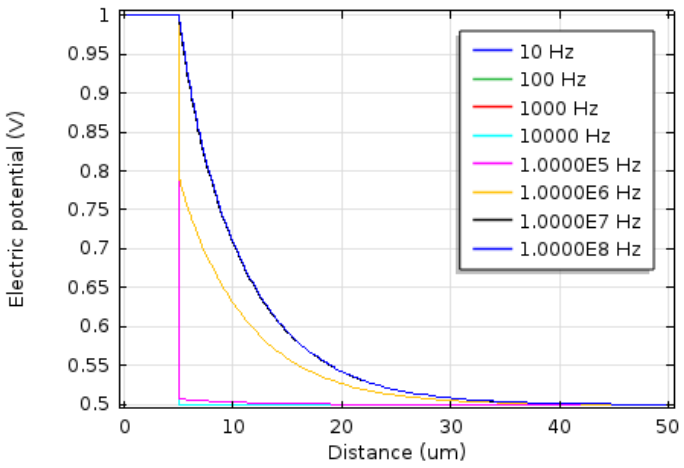

Figure 12.Comparison of the electric potential from substrate to the sea water from 10 to 10^8 Hz for 10 µm wide and 5 µm thick electrodes

Then the effect of the spacing of the electrodes on the penetration depth was simulated. Here 5 µm to 20 µm wide electrodes were simulated, where the spacing between the middle of the two electrodes was two times the width of the electrodes. The results in Figure 13 show the electrical potential across the 5 µm thick electrodes versus the distance from the substrate. The 1 V potential on the electrodes for the first 5 µm distance is consistent with the setup in the simulation. And it is clear that the penetration depth is proportional to the spacing between the centers of the two electrodes.

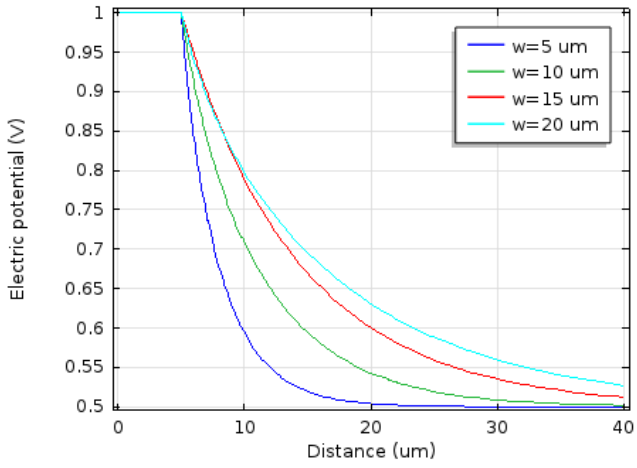

Figure 13. Electrical potential across the 5 µm thick electrodes versus the distance from the substrate for electrodes with different width at 10^8 Hz

3.3 Detection of Oil Droplets

As previously mentioned, 15 μm radius oil droplets show no degradation rate at a depth of 1000 meter to 2000 meter in the ocean [3]. Therefore, oil droplets with 15 μm radius were targeted for detection. And from before, we know the penetration depth is proportional to the electrodes spacing and enough penetration depth is needed to sense any change of electrical properties due to the presence of the oil droplets. Then for an oil droplet 20 μm away from the substrate, 30 μm wide electrodes were chosen to have enough penetration depth for detection. And the change of the admittance respect to the presence of oil droplets with different radius were investigated as a proof of concept for these interdigital sensors. The admittance change between 30 μm wide electrodes at frequencies between 10^3 and 10^8 Hz due to the presence of oil droplets with different radius at 20 μm away from the substrate were shown in Figure 14. It is obvious that the present of oil droplets changes the admittance between the electrodes at higher frequency. In addition, the admittances at higher frequencies are sensitive to the radius of the oil droplets as well. Moreover, the relationship between the size of the oil droplets and the change in admittance is not linear. Based on this simulation, electronics for admittance measurement at 10^6-10^7 Hz range with accuracy of 1.4 S across the interdigital electrodes will be needed to detect a single 15 μm radius oil droplet's presence inside the penetration depth of the interdigital electrodes. Here if the 30 μm wide interdigital electrodes are made into a 1 cm × 1 cm sensor, the penetration depth of 30 μm makes the total sensing volume to be 3×10^{-9} m^3. Then sensors' response to an oil droplet with 15 μm radius at 20 μm away makes the least detectable oil concentration to be 3.53×10^{-6}, namely 3.53 ppm. And the change in admittance is 1.4 S, which makes the sensitivity to

be 0.4 S/ppm. Since electronics to measure admittance with an accuracy of 1.4 S is available on the market, it is safe to say the limit of detection is 3.5 ppm, around 4 ppm. In addition, portable devices, such as SARK-110, have been commercially available to measure the complete impedance parameters at 10 MHz range, which suggests these interdigital oil droplets sensors can be integrated with electronics to be either put on autonomous underwater vehicles or deployed as separately modules.

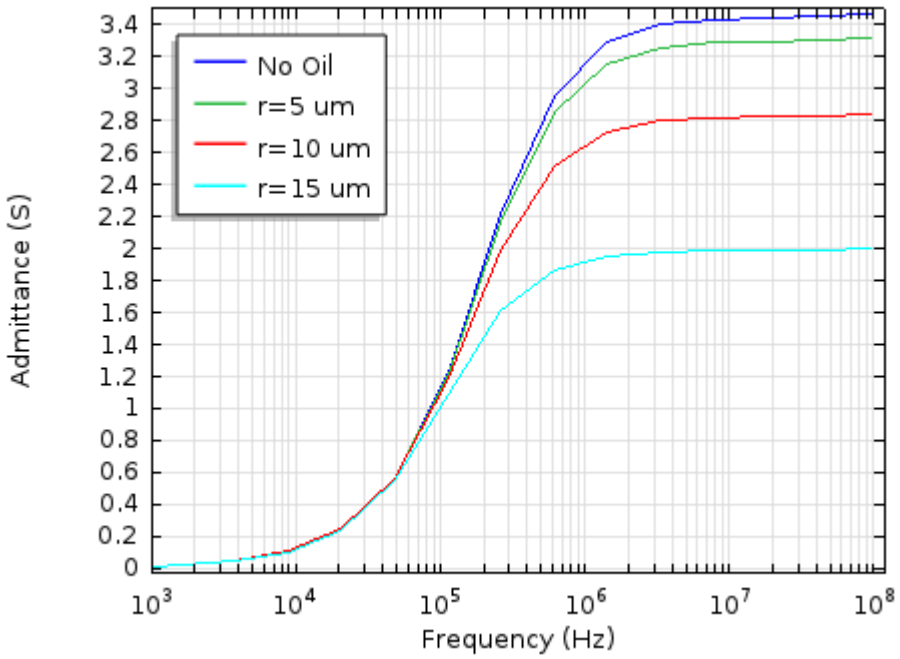

Figure 14. Comparison of the admittance between 30 µm wide electrodes due to the presence of oil droplets with different radius at 20 µm away from the substrate at frequencies between 10^3 and 10^8 Hz.

After the demonstration of the admittance change due to the presence of oil droplets with different sizes, the effects of the dielectric properties of the oil droplets were explored. Both oil droplets and water-in-oil emulsions were investigated. The relationship between the effective dielectric constant and the volume fraction of water in oil was calculated based on Equation 2.2 and plotted in Figure 15. Based on the volume fraction

of water, the effective dielectric constant varies from 2.5 to 78 as in Figure 15. To value the admittance change due to different effective dielectric constant, the corresponding effective dielectric constants of water-in-oil emulsions with 0%, 50%, and 100% volume fraction of water were found and cooperated into the simulation. The results, shown in Figure 16, suggest change in dielectric constant only change the admittance at higher frequencies a little. This suggests the admittance change from the presence of oil droplets come mostly from the resistance change in the bulk solution.

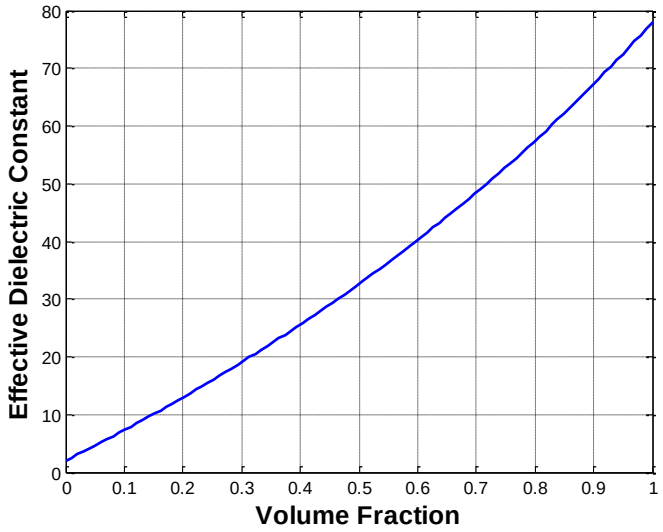

Figure 15. Effective dielectric constant of water-in-oil emulsions based on the volume fraction of the water in oil.

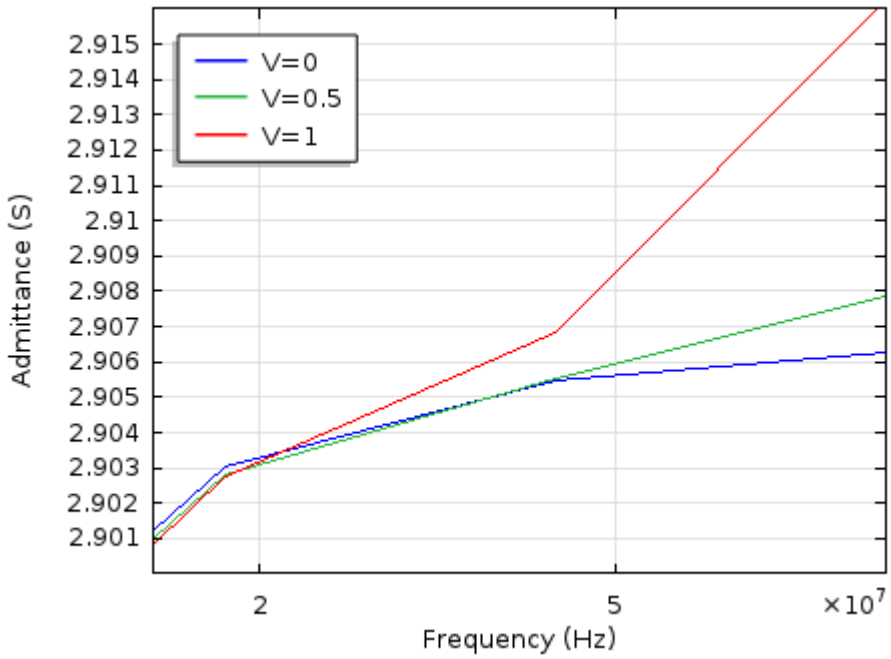

Figure 16. Comparison of the admittance between 30 µm wide electrodes responding to a 15 µm radius oil droplet with different volume fractions of water in oil at frequencies between 10^3 and 10^8 Hz.

Having demonstrated the admittance change and understood its origin, the sensor's performance based on the spacing of the electrodes and the position of the oil droplets respect to the electrodes were investigated. The investigation on spacing of the electrodes was done for detecting a 15 µm radius oil droplet 20 µm away from the substrates. As shown in Figure 17, the wider the electrode spacing, the more change in admittance at higher frequencies is present. And once the penetration depth, depends on the spacing of the electrodes, is comparable to the oil droplets' distance from the substrate, the change of admittance reduces.

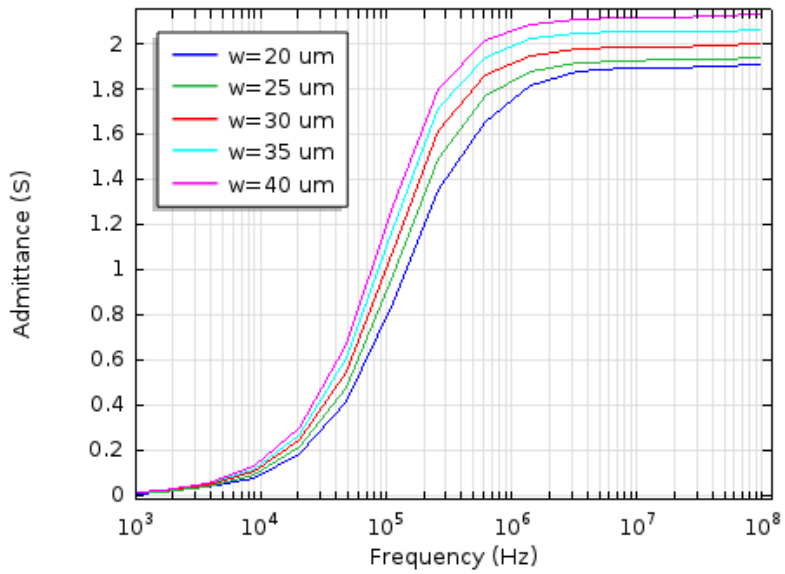

Figure 17. Comparison of the admittance between electrodes with different electrode width responding to a 30 μm oil droplet at 20 μm away from the substrates at frequencies between 10^3 and 10^8 Hz.

Then the admittance change due to the positions of the oil droplets was investigated. In this case, the electrode spacing was fixed to be 30 μm and the oil droplet had a radius of 15 μm. The admittance between electrodes at frequencies between 10^3 and 10^8 Hz is plotted in Figure 18. It is clear the presence of an oil droplet closer to the electrode will lead to a big change in admittance. And for the center of an oil droplet at a distance farther than the penetration depth, which is around 30 μm here, will only lead to a small change in the admittance between the electrodes.

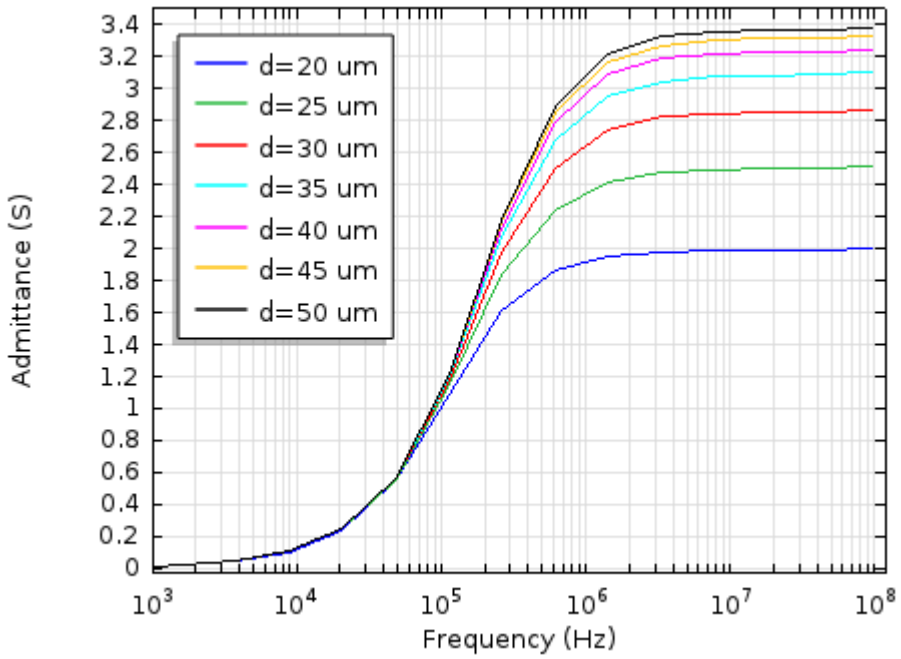

Figure 18. Comparison of the admittance between 30 μm wide electrodes responding to a 15 μm radius oil droplet at different distances away from the substrates at frequencies between 10^3 and 10^8 Hz.

After simulating the sensors' response to a single oil droplet, the presence of multiple oil droplets was studies. Here, the width of the electrodes was kept to be 30 μm, namely, with a penetration depth around 30 μm. And three oil droplets with a radius of 5 μm and a spacing of 15 μm were simulated separately, demonstrated in Figure 19. The results in Figure 20 shows the presence of different number of oil droplets will lead to different admittance changes at high frequency range. However, based on the location of oil droplets respect to the penetration depth, the magnitude of the effects on electrical signal are different. The disturbance of the electrical displacement field due to different amount of oil droplets was shown in Figure 21. From the distribution of the field lines, we can see how the introduced oil droplets perturb the field lines. And the further away the oil droplets are, the less perturbed the electric field is. Moreover, the multiple oil droplets

will lead to an admittance range between 2.9-3.2 S, which overlaps of the admittance range of 1.8 to 3.3 S due to the positioning of the a single oil droplet with identical radius.

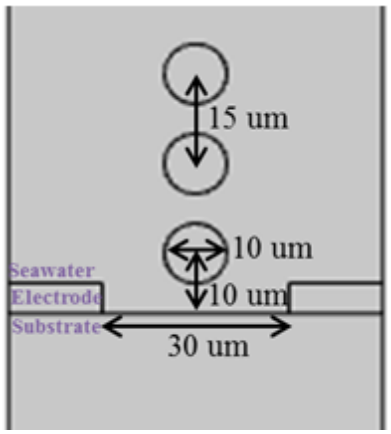

Figure 19. Geometric setup for three 5 µm radius oil droplets at different distances away from the 30 µm wide electrodes.

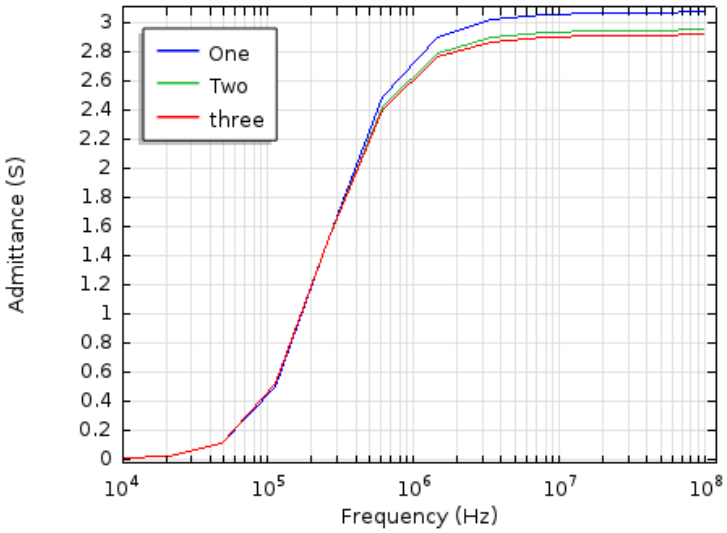

Figure 20. Comparison of the admittance between 30 µm wide electrodes responding to the present of three 5 µm radius oil droplets at different distances away from the electrodes at frequencies between 10^3 and 10^8 Hz.

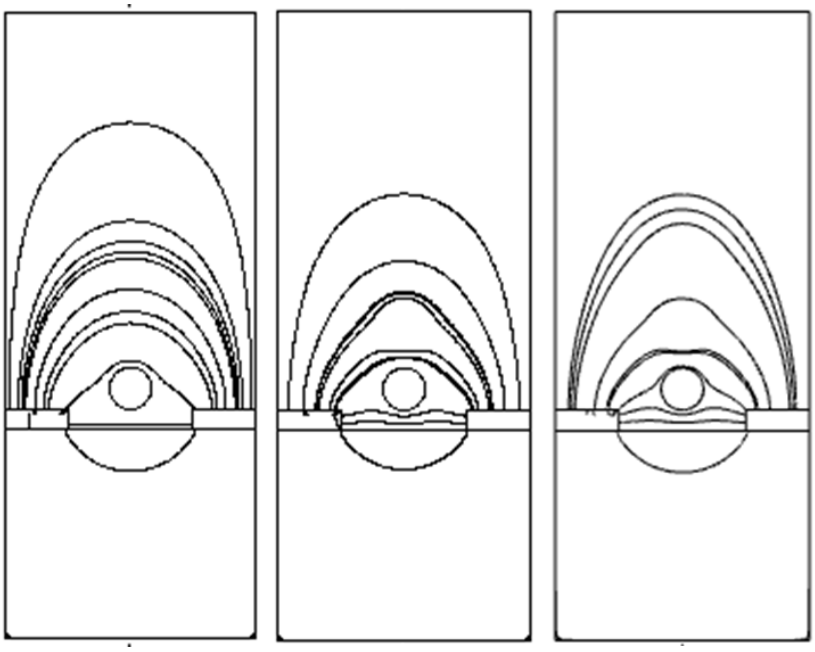

Figure 21. Comparison of the electrical displacement field in the sea water responding to the present of one (left), two (middle), and three (right) 5 μm radius oil droplets at 10^8 Hz.

3.4 Challenges and Proposed Solutions

Two of the major challenges for the micro electrodes sensor are surviving the corrosive environment and having selectivity. To be able to cope with the corrosive environment, platinum or carbon electrodes can be used due to their wide electrochemical stability windows. Meanwhile, parylene-C can be used to coat and protect electrodes made of other materials. Previous studies have shown parylene-C films, widely adapted in microsystem packaging, can provide an electrically insulating encapsulation for more than one year in saline solution [21]. In terms of selectivity, an absorbent can be introduced as a selective coating on top of the electrodes, shown in Figure 22. Aerogel shows great potential to be the material for this absorbent, since aerogel can absorb oil up

to 100 times its own weight withou absorbing water [22]. Moreover, a thin film of aerogel on interdigital gold electrodes has already been demonstrated as part of a humidity sensor [23]. For this interdigital oil droplets sensor, a layer of absorbent will be coated on the electrodes, and only crude oil, the gray area in the absorbent shown in Figure 22, can get into the detection range and alter the admittance. Moreover, the introduction of absorbent can reduce the power assumption of the system by changing from contiunous measurement to measurements from time to time.

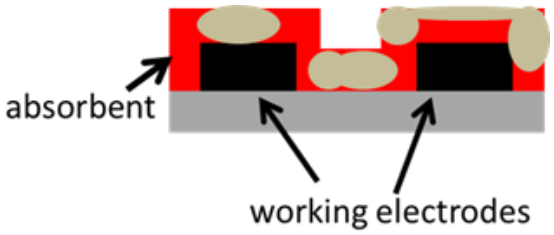

Figure 22. A layer of absorbent on top of the electrodes to increase the selectivity.

3.5 Conclusions

A model of interdigital sensor for oil droplets detection was established using AC/DC Module in COMSOL Multiphysics and verified by analytical solution. By using the model, the sensing range is found to be characterized by the penetration depth defined by the frequency of the signal and the spacing of the electrodes. Moreover, the admittance change between 30 μm wide electrodes at frequencies between 10^3 Hz and 10^8 Hz due to the presence of oil droplets with different radius at 20 μm away from the electrodes has demonstrated the feasibility of using interdigital sensor for oil droplets detection, where the limit of detection is 4 ppm. In addition, the effects of the electrode spacing, amount of oil droplets, and droplet size, position, and dielectric properties on the admittance between the electrodes at frequencies between 10^3 and 10^8 Hz have given design implications for this interdigital sensor. And the challenges of the corrosive environment and sensitivity are addressed at the end of the chapter. However, the change of admittance was observed to be affected by different parameters, such as the position, size, and amount of the oil droplets, which led to uncertainties in the measurements.

Chapter 4: Oil Droplets Manipulation

4.1 Oil Droplet Pre-Positioning Enabled by Acoustic Wave Field

Based on previous results, the position, size, and distribution of oil droplets all affect the admittance between the interdigital electrodes. Inspired by droplets manipulation in microfluidic application, an acoustic wave field enabled pre-positioning of the oil droplets was explored to eliminate the admittance's change due to position and distribution variation. Here, an established external pressure field of 1 bar at 1 MHz in the water was assumed. And the oil droplets will move under the acoustic radiation force generated by this acoustic field until they reach steady state and stayed in a preferential location in the acoustic field. Based on the density and sound velocity for water and oil samples found in literature, listed in Table 4, the density and sound velocity of oil droplets were chosen as 850 kg/m^3 and 1400 m/s respectively. The sizes of the oil droplets under study were from 10 μm to 100 μm, which satisfies the assumption that the particle size of interest has to be larger than momentum diffusion layer (0.6 μm) and smaller than the acoustic wavelength in water (1482 μm).

Sample	Density [kg/m^3]	Sound Velocity [m/s]
Water(distilled)	1000	1480
Light oil	810	1347
Medium oil	850	1401
Heavy oil	870	1441
Extra heavy oil	880	1480

Table 4. Density and Sound Velocity for Water and Oil Samples [24]

Firstly of all, the acoustic radiation force's distribution as a result of the pressure field on top of the electrodes was calculated and plotted in Figure 23. Here, acoustic

radiation force will move the oil droplets closer or farther from the electrodes. Based on the direction of the force, oil droplets were confirmed to move to the equilibrium points. And if there is only one equilibrium point within the penetration depth of the interdigital electrodes, all the oil droplets in the sensing range will be positioned at that specific distance above the electrodes, which will eliminate the admittance's change due to the position and distribution variation of oil droplets. And by using Equation 2.11, the maximum times oil droplets needed to move from a pressure node to the equilibrium point were calculated. The time's dependence on the size of the oil droplets are plotted in Figure 24. Based on this plot, droplets with a radius between 30 to 100 μm need only about 1 second to be positioned at the equilibrium point.

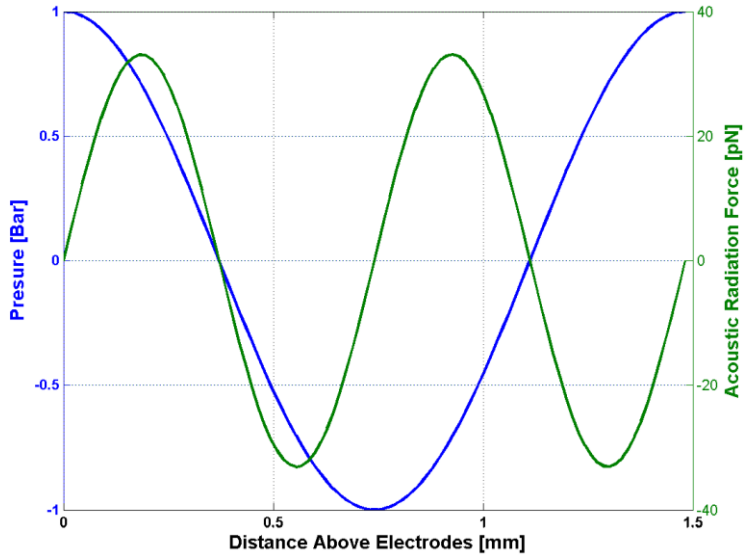

Figure 23. The pressure and acoustic radiation force on the particle at different positions.

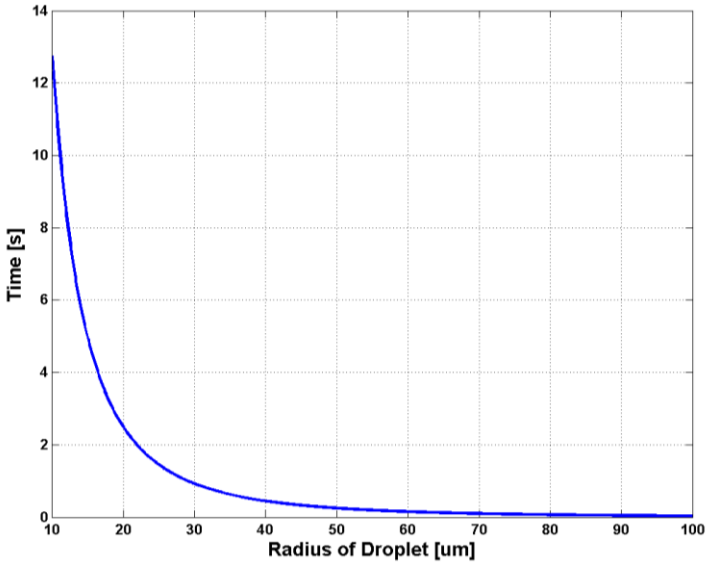

Figure 24. The maximum time oil droplets needed to move from a pressure node to the equilibrium point respect to the radius of oil droplets.

4.2 Validation of Simulation

Acoustic radiation force rise from the nonlinear effects in the pressure field, perturbation method is generally adapted to solve for the analytical solution. And similar idea was adapted for COMSOL Multiphysics simulation. First, the acoustic field was solved using the Pressure Acoustics Interface. The Particle Tracing for Fluid Flow interface was then used, where the acoustophoretic force was calculated based on the first order solution to acoustic field. And the Stokes' law is used to simulate the drag force, which is proportional to the dynamic viscosity, radius of the spherical object, and the flow velocity relative to the object. Considering both the acoustophoretic force and drag force on each individual particle, the movement of particles was simulated.

The solution from the COMSOL Multiphysics was first validated. Both the pressure field inside the water under a 1 MHz acoustic field and the acoustophoretic force on a 60 um polystyrene droplet suspended in the water were compared to analytical

solution. As shown in Figure 25, the simulation results of the pressure field and acoustophoretic force are very consistent with the analytical results and make COMSOL Multiphysics a reliable tool for device design.

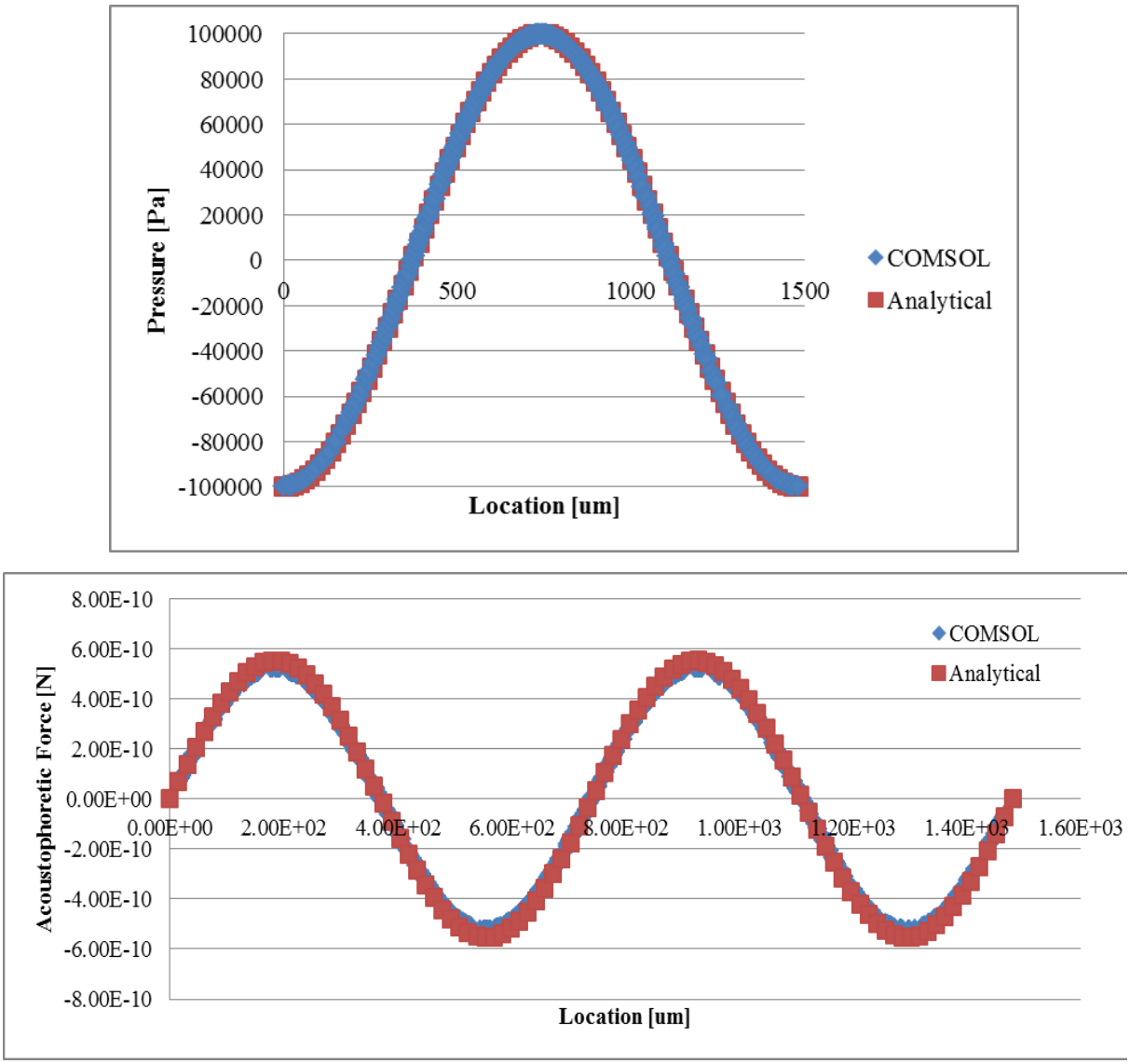

Figure 25. The pressure field inside the water on top of a 1 MHz acoustic field (up) and the acoustophoretic force on a 60 um polystyrene droplet suspended in the water (down).

Then the capacity of the simulation was explored with the same system, where polystyrene particles (ρ = 1.05 g/cm3 and $\beta = 2.46 \times 10^{-10}$ Pa^{-1}) were suspended in water (ρ = 1 g/cm^3 and $\beta = 4.55312.46 \times 10^{-10}$ Pa^{-1}) under a 1 MHz 1 bar acoustic pressure. As

shown in Figure 26, evenly distributed particles were generated and experiencing only acoustophoretic force and drag force at time 0 s. And within 0.5 second, all the polystyrene particles moved to the equilibrium point. This simulation shows the promise of using acoustic pressure field to position particles and using COMSOL Multiphysics as a design tool for such system. However, some residual particles were presented, which showed the limitation of this method to pre-position droplets in an acoustic wave field.

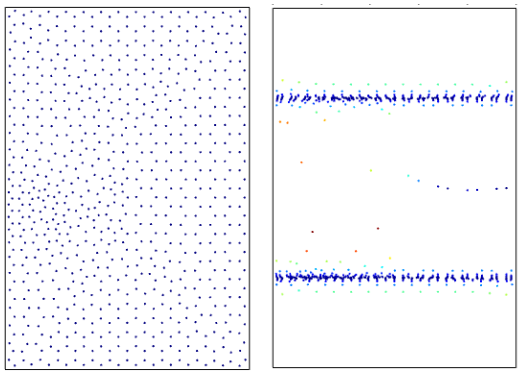

Figure 26. Evenly distributed particles were generated and subject to acoustophoretic and drag forces at 0 s (left). Within 0.5 second, polystyrene particles moved to the equilibrium point (right).

In another set of simulation, particles were released with an initial velocity from an inlet at 0 second. Under the influence of the acoustophoretic force and drag force, particles first moved to the equilibrium point and then kept moving along the line with a steady state velocity. The results extracted from the particle trajectories for each frame were shown in Figure 27. It was clear that the accelerations at difference locations were different, which was consistent with the analytical solution to the acoustophoretic force.

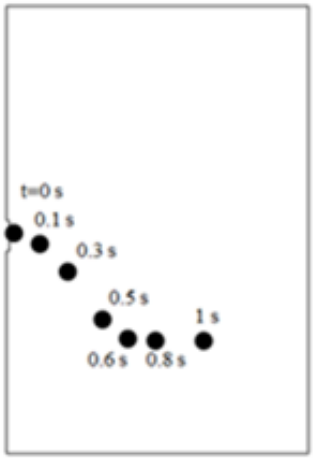

Figure 27. Particles released with an initial velocity from an inlet at 0 second first moved to the equilibrium point and then kept moving along the line with a steady state velocity

4.3 Conclusions

An acoustic wave field enabled oil droplets pre-positioning was explored to eliminate the admittance's change due to position and distribution variation of the droplets. The calculation of the acoustic radiation force and the maximum time oil droplets needed to move from a pressure node to the equilibrium point have shown promise for pre-positioning micro scale oil droplets in an external pressure field of 1 bar at 1 MHz. Moreover, simulation of 60 μm polystyrene droplets suspended in the water in COMSOL Multiphysics was established and verified, which demonstrated COMSOL Multiphysics to be a reliable tool for device design in the future.

Chapter 5: Conclusion and Future Work

5.1 Conclusion

This work has proposed and demonstrated micro scale interdigital sensors with acoustic pre-positioning for oil droplet detection with a simulated limit of detection of around 4 ppm. 30 μm wide electrodes sensing at frequencies between 10^3 and 10^8 Hz showed the ability to detect the presence of micro scale oil droplets at 20 μm distance away. The effects of the electrode spacing, amount of oil droplets, and droplet size, position, and dielectric properties on sensor performance were characterized, which gave some design implications. In addition, an acoustic wave field enabled pre-positioning of oil droplets showed the potential to eliminate the change in admittance due to the position and distribution variation of oil droplets. The schematic of the proposed interdigital sensor with an acoustic wave field for oil droplets pre-positioning is shown in Figure 28. This device shows great promise for long-duration monitoring of oil droplets and water-in-oil emulsions, which can be implemented in sensor networks in the ocean for high temporal and spatial resolution applications.

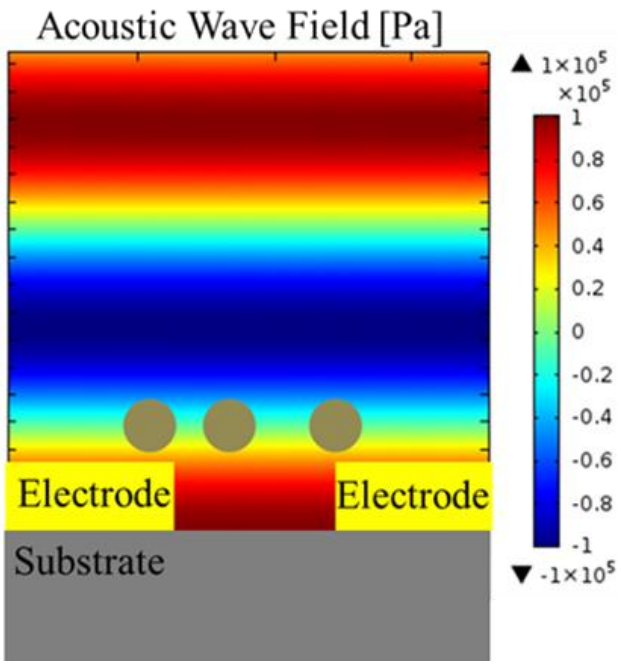

Figure 28. Schematics of the proposed interdigital sensor with an acoustic wave field for oil droplets pre-positioning.

5.2 Future Work

First of all, the fabrication process of the interdigital sensors will be finalized. Carbon and platinum electrodes are going to be fabricated and characterized. The tested results will be compared with the analytical solution and simulation. At the same time, interdigital sensors' real time response to the presence of oil droplets will be tested. In addition, the COMSOL simulation for pre-positioning micro scale oil droplets in a pressure field of 1 bar at 1 MHz will be done to aid the device design. And the effects of the turbulent flow and ocean currents in an open ocean environment on oil droplets will be investigated.

Bibliography

[1] Oil in the Sea III: Inputs, Fates, and Effects, Washington, DC: The National Academies Press, 2003.

[2] ITOPF, "Fate of Marine Oil Spills," Impact PR & Design Limited, Canterbury, UK, 2011.

[3] Elizabeth W North, E Eric Adams, Anne Thessen, Zachary Schlag, Ruoying He, Scott Socolofsky, Stephen Masurani, and Scott Pechham, "The influence of droplet size and biodegradation on the transport of subsurface oil droplets during theDeepwater Horizon spill: a model sensitivity study," *Environmental Research Letters*, no. 10, p. 024016, 2015.

[4] W. Hehr, "Review of modeling procedures for oil spill weathering behavior," in *Oil Spill Modeling and Processes*, Southampton, UK, WIT Press, 2001, pp. 51-90.

[5] M. Fingas, "Oil Spill Remote Sensing: A Review," in *Oil Spill Science and Technology*, Elsevier, 2011, pp. 111-158.

[6] Zhengkai Li, Kenneth Lee, Paul E. Kepkey, Ole Mikkelsen, and Chuck Pottsmith, "Monitoring Dispersed Oil Droplet Size Distribution at the Gulf of Mexico Deepwater Horizon Spill Site," in *International Oil Spill Conference*, 2011.

[7] "Tracking a Tail of Oil Droplets," *Oceanus Magazine,* 17 September 2010.

[8] Kenneth Lee, Jerry Neff, "Measurement of Oil in Produced Water," in *Produced Water*, New York Dordrecht Heidelberg London, Springer, 2011, pp. 57-88.

[9] John Heidemann, Milica Stojanovic, and Michele Zorzi, "Underwater Sensor networks: applicatoin, advances and challenges," *Philosophical Transactions of The Royal Society,* no. 370, pp. 158-175, 2012.

[10] Mohamed N, Jawhar I, Al-Jaroodi J, Zhan, "Sensor Network Architectures for Monitoring Underwater Pipelines," *Snesors,* vol. 11, no. 11, pp. 10738-10764, 2011.

[11] Kamrul Hakim Sudharman K Jayaweera, "Source localization and tracking in a dispersive medium using wireless sensor network," *EURASIP Journal on Advances in Signal Processing,* p. 147, 2013.

[12] J. Verba, "3D numerical simulations and measurements of effective dielectric properties of oil-in-water emulsions," in *Electromagnetics REsearch Symposium*, Stockholm, 2013.

[13] Levy, O., Stroud, D, "Maxwell Garnett theory for mixtures of anisotropic inclusions: Application to conducting polymers," *Physical Review B,* vol. 56, no. 8035, p. 13, 1997.

[14] Cox, R. A., McCartney, M. J. & Culkin, F, *Deep Sea Res*, vol. 17, no. 34, pp. 679-689, 1970.

[15] W. Olthuis, W. Streekstra, P. Bergveld, "Theoretical and experimental determination of cell constants of planar-interdigitated electrolyte conductivity sensors," *Sensors and Actuators B,* pp. 252-256, 1995.

[16] B. J. Kirby, Midro- and Naoscale Fluid Mechanics, Cambridge University Press, 2010.

[17] John Newman and Karen E. Thomas-Alyea, Electrochemcical Systems, John Wiley & Sons, Inc., 2004.

[18] Xiaobei B. Li, Sam D. Larson, Alexei S. Zyuzin, and Alexander V. Mamishev,, "Design Principles for Multicuhannel Fringing Electric Field Sensors," *IEEE Sensors Journal,* vol. 6, no. 2, pp. 434-440, 2006.

[19] Mikkel Settnes and Henrik Bruus, "Forces acting on a small particle in an acoustical field in a viscous fluid," *Physical Review E,* vol. 85, no. 1, p. 016327, 2012.

[20] J. Guo, Y. Chen, Y. Kang, "RF-activated surface standing acoustic wave for on-chip controllably aligning of bio-microparticles," in *Microwave Workshop Series on RF and Wireless Technologies for Biomedical and Healthcare Applications (IMWS-BIO), 2013 IEEE MTT-S International*, Singaopre, 2013.

[21] Jui-Mei Hsu; Rieth, Loren; Normann, R.A.; Tathireddy, P.; Solzbacher, F, "Encapsulation of An Intergrated Neural Interface Device with Parylene C," *IEEE TRANSACTIONS ON BIOMEDICAL ENGINEERING,* vol. 56, no. 1, pp. 23-29, 2009.

[22] Qifeng Zheng, Zhiyong Cai, and Shaoqin Gong, "Green synthesis of polyvinyl alcohol (PVA)–cellulose nanofibril (CNF) hybrid aerogels and their use as superabsorbents," *Journal of Materials Chemistry,* no. 2, pp. 3110-3118, 2014.

[23] Chien-Tsung Wang, Chun-Lung Wu, I-Cherng Chen, Yi-Hsiao Huang, "Humidity sensors based on silica nanoparticle aerogel thin films," *Sensors and Actuators B: Chemical,* vol. 1071, no. 1, pp. 402-420, 2005.

[24] R. J. Kalivoda, "Understanding the limits of ultrasonics for crude oil measurement," FMC Technologies, Erie, Pennsylvania, USA.